



HAL
open science

On the collapse pressure of armored bubbles and drops

Olivier Pitois, M.. Buisson, Xavier Chateau

► **To cite this version:**

Olivier Pitois, M.. Buisson, Xavier Chateau. On the collapse pressure of armored bubbles and drops. *European Physical Journal E: Soft matter and biological physics*, 2015, 38 (5), pp.48. 10.1140/epje/i2015-15048-9 . hal-01189021

HAL Id: hal-01189021

<https://hal.science/hal-01189021>

Submitted on 1 Sep 2015

HAL is a multi-disciplinary open access archive for the deposit and dissemination of scientific research documents, whether they are published or not. The documents may come from teaching and research institutions in France or abroad, or from public or private research centers.

L'archive ouverte pluridisciplinaire **HAL**, est destinée au dépôt et à la diffusion de documents scientifiques de niveau recherche, publiés ou non, émanant des établissements d'enseignement et de recherche français ou étrangers, des laboratoires publics ou privés.

On the collapse pressure of armored bubbles and drops

O. Pitois*, M. Buisson and X. Chateau,

*Université Paris Est, Laboratoire Navier, UMR 8205 CNRS – École des Ponts ParisTech – IFSTTAR
cité Descartes, 2 allée Kepler, 77420 Champs-sur-Marne, France*

Abstract:

Drops and bubbles wrapped in dense monolayers of hydrophobic particles are known to sustain a significant decrease of their internal pressure. Through dedicated experiments we investigate the collapse behavior of such armored water drops as a function of the particle-to-drop size ratio in the range 0.02-0.2. We show that this parameter controls the behavior of the armor during the deflation: at small size ratios the drop shrinkage proceeds through the soft *crumpling* of the monolayer, at intermediate ratios the drop becomes *faceted*, and for the largest studied ratios the armor behaves like a *granular arch*. The results show that each of the three morphological regimes is characterized by an increasing magnitude of the collapse pressure. This increase is qualitatively modeled thanks to a mechanism involving out-of-plane deformations and particle disentanglement in the armor.

*corresponding author: olivier.pitois@ifsttar.fr

Tel.: 33 1 81 66 84 51

1. Introduction

Hydrophobic particles can serve as stabilizers for emulsions [1] and foams [2-5]. Those particles adsorb at the surface of drops or bubbles, providing exceptional stability properties against coalescence and Ostwald ripening [6,7], or drying [8,9]. The accepted picture for such a stabilizing effect involves the formation of a dense particle monolayer around the drop or the bubble, i.e. a solid *armor*. Whereas the stability of those systems has been considerably investigated, the mechanical behavior of the armor remains to be understood in details, as evidenced by the existence of several distinct approaches for describing this behavior. These approaches are inspired either by studies on surfactant monolayers (Langmuir isotherms) [9-12], or by thin elastic sheets [13-15], or they are based on micro-capillary models [11,16-18]. One can expect that experiments will contribute to understand all the specific features of these complex solid/fluid interfaces. To this regard, several studies have been performed on particle rafts under compressive stress. The onset of wrinkling patterns has been reported as well as the collapse of the monolayer above a critical stress, whose magnitude is comparable to the surface tension of the nude interface [11,19]. Besides, experiments performed on armored millimeter drops characterized by a small particle-to-drop size ratio, i.e. 0.01, indicate that their relative capillary pressure can be decreased down to zero before to observe their collapse [19]. It was also reported that before the collapse, the armor exhibits a crumpled aspect [19]. On the other hand, numerical simulations for armored bubbles characterized by a larger size ratio, i.e. ≈ 0.1 , show that those armors become faceted and that the corresponding relative collapse pressures can be negative [18]. Moreover, calculations on ideal armors indicate that highly negative relative collapse pressures can be obtained if the number of involved particles is small [16]. These results suggest that for armored drops (or bubbles) there exists a strong

dependence of the collapse pressure on the size ratio. To our knowledge, such dependence is not reported in literature.

In this paper, we investigate experimentally the mechanical strength of armored water drops characterized by particle-to-drop size ratios varied in the range 0.02-0.2. As shown in the following, the results reveal the effect of the size ratio on both the collapse pressure and the morphology of the collapsing drop, providing a consistent link between previous results obtained within distinct narrow ranges of the size ratio.

2. Experimental

The experimental setup has been designed to measure the collapse pressure of armored drops within imposed pressure conditions. A hemispherical drop of water (Millipore 18,2 M Ω .cm) is formed at the apex of a cylindrical PTFE tip. Several tips are used in order to vary the radius R of the drop in the range 0.225 – 1.125 mm. The tip holder is connected to a water reservoir in such a way that the liquid pressure in the drop is set by the height ΔH separating the drop from the liquid level in the reservoir (see Fig. 1). The latter is accurately controlled by removing or by adding water volumes with a syringe-pump. The drop is placed under the objective of a microscope equipped with fluorescence optics (Top view in Fig. 1). Another view (Side view in Fig. 1) of the drop is obtained with a camera equipped with a zoom. The top view is used to follow the evolution of the particle monolayer at the drop surface. The side view is rather used to check that the initial shape of the armored drop is hemispherical. Particles are fluorescent (Ex 468/Em 508 nm) polystyrene microspheres provided by Duke Scientific Corporation (dry particles). Their radius is $a = 16 \mu\text{m}$ and $a = 40 \mu\text{m}$, and their standard deviation $\Delta a/a$ is less than 10%. Their density is 1.05. The procedure for the measurement can be described as follows. A suspension is prepared beforehand with the

particles and a mixture composed of ethanol and water (20/80). A hemispherical water drop is formed in equilibrium with the liquid pressure in the reservoir. Then the connection between the drop and the reservoir is closed by a valve and a small amount of the particle suspension is deposited on the drop surface using a micropipette. The valve is necessary to prevent the influx of water from the reservoir induced when the alcohol enters the drop and reduces the surface tension. By waiting for several minutes, the alcohol evaporates from the drop surface, which allows for the hemispherical drop shape to be restored when the valve is reopened. Note that this procedure intrinsically guarantees that alcohol has left before starting the measurement (if surface tension is reduced by the presence of alcohol, the drop will be swept away by water influx from the reservoir). The desired starting configuration is a hemispherical drop covered with a homogeneous particle layer with no surface pressure, i.e. the effective surface tension of the armored drop is equal to the surface tension σ of the particle-free drop (0.07 N/m). It is not easy to obtain this starting configuration because this requires depositing the right amount of particles for the hemispherical shape. If it is too small, there will be an empty space at the apex of the drop (the particles settle at the vertical surface of the drop), and a significant surface reduction will be required before to measure the mechanical response of the homogeneous monolayer, which will impact the subsequent measurement. If the amount of particles is too large, the monolayer will undergo a significant stress that also will impact the subsequent measurement. In practice, several small amounts of particle suspension are deposited successively until the desired starting configuration is obtained. Then, the initial drop pressure P_{drop}^0 is reduced to P_{drop} in a quasi-static way. In the following, we refer to the pressure difference $\Delta P_{drop} = P_{drop}^0 - P_{drop}$. The syringe-pump is used in withdrawing mode at a volume flow rate Q . The liquid level in the reservoir is lowered and the drop pressure decreases accordingly to the rate: $dP/dt = -\rho g Q/S$, where S is the cross-sectional area of the reservoir ($S \approx 3 \text{ cm}^2$). The typical rate is $dP/dt \approx -0.2 \text{ Pa/s}$,

which corresponds to quasi-static conditions (we have not observed appreciable changes of the results when the rate was decreased by a factor 5). Note that during the measurement, water evaporation from the drop surface is continuously compensated by the water influx from the reservoir without appreciable change in liquid pressure thanks to the large value of S . Images of top and side views are grabbed during the pressure decrease until the drop collapse is observed at $\Delta P_{drop} = \Delta P_{collapse}$.

3. Results

Pictures presented in Fig. show deviations in the contact angle of particles before any pressure decrease, as well as deviations in the particle size (within the expected range). Due to those defects, the particle centers are not perfectly positioned on a spherical surface and the local curvature of the armor is not constant locally. The average contact angle is estimated to be equal to 30° - 40° . It appears that those defects in the armor's curvature accentuate during the pressure decrease, which seems to cause the drop collapse. However, the evolution of the drop's morphology clearly depends on the size ratio, as shown by the comparison of Fig. 2a, 2b and 2c. From the pictures, one can classify the collapse behavior into three regimes. For $a/R \approx 0.05$, the defects initiate numerous inward buckling events, each on a length scale corresponding to roughly ten particles. Clearly, at this stage, those local inversions in the armor's curvature are not spread enough in order to induce the collapse of the drop which remains in mechanical equilibrium within the imposed pressure conditions. In approaching the collapse pressure, the aspect of the armor becomes more irregular, or *crumpled*. Generally, a large inward buckling, i.e. with size of the order of R , eventually develops from one of the previously described local defects (Fig. 2a). Note that such a buckled drop can sustain further pressure decrease before collapsing. For $a/R \approx 0.1$, the behavior of the drop is different: the

armor is less crumpled and exhibits a *faceted* shape. The collapse of the drop occurs through the buckling of one of the facets, whose size is generally of the order of R , i.e. ten particles (Fig. 2b). The faceted regime corresponds to a stable mechanical equilibrium, as already mentioned in [18]. For $a/R \approx 0.15$ the faceted regime is no more observed. The armor resembles an arch whose shape is almost unchanged until one particle suddenly moves inwards and induces the rapid collapse of the drop (Fig. 2c). Thus, each value of a/R is characterized by a given armor morphology before the collapse. As shown in the following, each value of a/R is also characterized by a dedicated value of the collapse pressure.

Results for the collapse pressure difference $\Delta P_{collapse}$ are presented in Fig 3 as a function of a/R . $\Delta P_{collapse}$ can be compared directly to the capillary pressure of the initial drop, i.e. $2\sigma/R$ (dashed line on Fig. 3). $\Delta P_{collapse} \lesssim 2\sigma/R$ for $a/R \lesssim 0.07$, which means that the collapse occurs as the drop capillary pressure becomes small but positive. This is in quantitative agreement with previous results obtained by Monteux et al. [19] with millimeter drops covered with micrometer-sized particles [], i.e. $a/R \ll 1$. As $a/R > 0.07$, the collapse pressure exceeds $2\sigma/R$, which means that the drop reaches negative capillary pressures before the collapse. Note that the deviation $\Delta P_{collapse} - 2\sigma/R$ reaches values of the order of $2\sigma/R$ as a/R increases up to 0.2. Experiments performed with another particle size (32 μm) show the same behavior, although the transition $\Delta P_{collapse} \approx 2\sigma/R$ is observed at a slightly smaller value for a/R , i.e. 0.03. We suggest that this deviation originates from the difference in contact angle for the two particle sizes, but this point remains to be understood. These results clearly show that the particle monolayer develops surface forces that can maintain the spherical drop shape in the absence of positive capillary pressure, and can even sustain significant negative capillary pressures, as expected by Kam & Rossen for rigid 2D granular shells [16].

It is interesting to compare our data with numerical results obtained by Abkarian et al. [18]. In that paper, the authors have not reported explicitly the collapse pressure, but the latter can be deduced from the curves $\Delta P/\Delta P_L = f(V/V_p)$ on Fig. 2 of the reference [18] as well as in the complementary material of the same reference. We deduce the following values [Note1]: $\Delta P_{collapse}/(2\sigma/R) \simeq 1.57, 1.33$ and 1.39 for $a/R \simeq 0.09, 0.17$ and 0.23 respectively. Those data are reported in Fig. 4 for comparison with our data. Domains identified for the ‘crumpled’, ‘facets’ and ‘arch’ regimes are presented. Experimental results obtained by Monteux et al. [19] for $a/R \ll 1$ are also reported for comparison. It appears that the present experimental results, which cover a large range of a/R values, are consistent with previously reported collapse pressures for $a/R \ll 1$ [19], characterized by $\Delta P_{collapse}/(2\sigma/R) \leq 1$, as well as for $a/R \approx 0.1$ [18], characterized by $\Delta P_{collapse}/(2\sigma/R) > 1$.

4. Discussion

The collapse of spherical shells is an old problem in elastic theory. It is known that the spherical shape is unstable for pressures larger than the critical pressure $P_C = 4\sqrt{\kappa E_{2d}}/R^2 = 4E_{2d}t/R^2$ [20], where $E_{2d} = E_{3d}t$ is the two-dimensional Young modulus (E_{3d} and t are respectively the bulk modulus and the thickness of the shell) and $\kappa = E_{3d}t^3 = E_{2d}t^2$ is the bending rigidity of the shell (the unities of E_{2d} and κ are respectively N m^{-1} and N m). Note that we performed calculations with a FEM software (Castem) in order to validate the expression of P_C for hemispherical elastic shells. In order to compare our experimental data with P_C , one has to evaluate κ and E_{2d} . Previous experiments on horizontal particle rafts have provided estimations for these parameters: $1 \lesssim E_{2d}/\sigma \lesssim 2$ [13] and $0.5 \lesssim \kappa/\sigma a^2 \lesssim 1.5$ [15]. The theoretical collapse pressure is estimated from the ranges of values for E_{2d} and κ , which gives $1.4a/R \lesssim P_C/(2\sigma/R) \lesssim 3.5a/R$. The upper bound is reported in Fig 4, showing that

the theoretical values deduced from the elastic theory underestimate the measured collapse pressures of armored drops. Note that a best fit of the data gives $P_c/(2\sigma/R) \approx 11a/R$ (expressed in terms of the two-dimensional elastic modulus, it gives $E_{2d} \approx 3\sigma \approx 0.2 \text{ N m}^{-1}$). Although the analogy with conventional elastic sheets is manifest, this behavior remains to be understood in terms of the mechanics at the scale of the grains. For example, one has to justify such a small value for E_{2d} whereas the Young modulus of the particles is large ($E \sim 10^9 \text{ Pa}$). Indeed, the studied armored interfaces were dense and under compressive stress we didn't notice significant in-plane densification due to particle motions. This is especially true for the armored drops in the arch regime, where in-plane densification is expected to result only through the deformation of contact areas between particles. The estimation of E_{2d} in this regime provides values that are at least three orders of magnitude larger than 0.2 N m^{-1} [Note2]. On the other hand, our observations revealed that well-beyond the onset of collapse particle, overlapping, i.e. accordion pattern, develops and could contribute to weaken the particle monolayer when subjected to in-plane compressive stress. In order to discuss further this effect, we propose the following simple modeling elements.

First of all, deviations in particle radius (δa) and in contact angle ($\delta\theta$) are assumed to induce geometrical disorder with regard to particle positions perpendicular to the mean plan of the monolayer: $\delta h/a = (\delta a/a)\cos\theta - \delta\theta\sin\theta$. Note also that the particle configuration in the plan of the monolayer could also induce deviations $\delta h/a$ during the pressure reduction because all the particles do not undergo the same displacement with reference to the liquid/gas interface [18]. For the sake of simplicity, we describe the geometrical disorder using a single global parameter $\delta h/a$ that incorporates all the above-mentioned effects, whatever may be the contribution of each one. Equivalently, the geometrical disorder can be described using the overlapping angle φ (Fig. 5a).

Whereas particle rafts are known to yield through wrinkling patterns, the development of such deformation modes is initially prevented for bubbles and drops due to their capillary pressure. However, as the internal pressure decreases significantly, inwards buckling becomes possible in involving deformations over a length scale of the order of the radius of the drop R [19]. Therefore, before reaching such a level of pressure decrease, the main deformation mechanism is the particle overlapping mechanism induced by the geometrical deviations $\delta h/a$, as depicted in Fig. 5b.

For monolayers characterized by a small a/R ratio, particle overlapping due to the increase of the surface stress results in the densification of the monolayer, i.e. the reduction in surface area, so that a two-dimensional Young modulus can be defined. Note that restoring capillary forces develop as the liquid-gas interface distorts around the particles that are moved perpendicular to the plan of the monolayer. The simplest way to model this effect is to assume that the restoring force takes the form: $F_{rest} \simeq k(a)\sigma d$, where $k(a)$ is a geometrical constant and d is the interface distortion. Note that this expression is compatible with the case of a single sphere attached to a liquid/gas interface and moved away from this interface [21-23], where $k \approx 1$ for the particle size considered in this study, keeping in mind that the present configuration is much more complicated. Any bulk pressure reduction (with respect to the capillary pressure) induces an increase of the surface pressure $-\Pi$ (by convention $\Pi < 0$ for compressive stress) in the plane of the monolayer, in such a way that the mechanical equilibrium of the armored drop is maintained, i.e. $\Delta P_{drop} = -2\Pi/R$ [16]. Equivalently, an effective surface tension $(\sigma + \Pi) < \sigma$ can be defined. In neglecting the friction at contact between the particles as well as the drop curvature, the mechanical equilibrium of such a distorted particle monolayer (see the periodic particle element in Fig. 5b) is ensured if $k\sigma d \approx -\Pi a \tan \varphi^*$, where the angle φ^* describes the orientation of contact forces with respect to the mean plan of the monolayer. φ^* accounts for the particle overlapping during

the increase of the surface pressure, i.e. $\sin \varphi^* = \delta h/a + d/a$. According to this equilibrium, the relation between the surface pressure and φ^* is $-\Pi/k\sigma \approx \cos \varphi^* (1 - (\delta h/a)/\sin \varphi^*)$. Then, in considering a model particle raft structured with the geometrical element of Fig. 5b, i.e. accordion-shaped particle raft, any increase in surface pressure can be related to the relative reduction in the raft length $\Delta L/L \approx \cos \varphi^*/\cos \varphi - 1$, which allows defining a surface elastic modulus (secant modulus) $E_{2d} = \Pi/(2\Delta L/L)$. For deformations of the order of -0.1 and $\delta h/a \approx 0.1$, $E_{2d} \approx 10k\sigma$. The constant k is expected to be of order unity and the estimation for E_{2d} indeed corresponds to soft materials, whose apparent modulus scales with σ , which is consistent with experimental results obtained on particle rafts [13].

As the ratio a/R increases, the crumpled morphology lessens and the drops become more faceted during the pressure reduction. This can be explained by the fact that the drop curvature counterbalances the effect of the geometrical disorder, so that local inward buckling is prevented. More precisely, the inversion of the local curvature locks when $\delta h/a < 2a/R$ (see Fig. 5c). In this regime, the inward buckling of the drop proceeds by pushing some particles away from the center of the drop in order to release some space within the monolayer, which allows for buckling facets to form. In the simulations by Abkarian et al. [18], topological defects, the 12 fivefold disclinations in the ordered particle monolayer, serve as vertices for buckling facets of size R . In our experiment, less symmetric buckled structures were observed, but however the characteristic size of the facets is R . It is worthwhile to recall that the faceted regime was found to correspond to a narrow range of a/R values.

In carrying on with the model, we now focus on the increase of the reduced collapse pressure as a function of a/R . The starting point is the idea that for $\delta h/a < 2a/R$, the inward buckling of the drop is initiated by disentanglement events involving at least one particle. As

described above, this is achieved by pushing several particles outward of the drop surface, over a distance d , in order to release the space required for this disentanglement. According to the approach proposed above, the surface pressure required to obtain such interfacial distortion is $-\Pi \approx kd\sigma/(\delta h + d)$. Besides, the disentanglement of a particle is allowed when the upward motion of its neighbor corresponds to $d \approx a^2/R$, which involves a reduced collapse pressure equal to $\Delta P_{collapse}/(2\sigma/R) \equiv -\Pi/\sigma \approx k(a/R)/(\delta h/a + a/R)$. This increasing function of a/R is in qualitative agreement with our experimental data. Note that as a/R increases up to 0.2 buckling facets cannot be clearly defined anymore as they involve only two or three particles. In that case, the armor is a strong granular arch for which any disentanglement event causes the instantaneous collapse of the drop. Those situations tend towards the ideal situation considered by Kam & Rossen [16], although for the latter case the critical pressure corresponds to the invasion of the liquid/gas interface through the porosity of the armor, i.e. $\Delta P_{collapse}/(2\sigma/R) = 6/(a/R)$, which is at least one order of magnitude larger than the measured collapse pressures.

5. Conclusion

We measured the collapse pressure of water drops armored with hydrophobic particles as the particle/drop size ratio increases in the range 0.02-0.2. We observed three distinct morphological regimes when the drop pressure was decreased within quasi-static conditions: at small size ratio, numerous local inward buckling events occur and the armor has a crumpled aspect; in contrast, for the largest size ratios, the armor looks like a spherical granular arch and sustains the pressure reduction without any significant particle motion; for intermediate size ratio, the armor's shape is faceted. Each of those morphologies has been found to correspond to a dedicated level for the collapse pressure: whereas at small size ratio

the drop collapses when its capillary pressure gets close to zero, significant negative capillary pressures are measured for the largest size ratios and intermediate collapse pressures characterize the faceted regime. Observations have revealed that the collapse is initiated by intrinsic geometrical defects. The effects of those defects are partly counterbalanced by the drop curvature, and the relative increase of the armor's strength can be understood from a simple mechanism involving the disentanglement of particles that form the granular armor.

References

- [1] S. U. Pickering, *J. Chem. Soc.*, 1907, **91**, 2001-2021.
- [2] R. G. Arlagova, D. S. Warhadpande, V. N. Paunov and O. D. Velev, *Langmuir*, 2004, **20**, 10371-10374.
- [3] B. P. Binks and T. S. Horozov, *Angew. Chem., Int. Ed.*, 2005, **44**, 3722-3725.
- [4] U. T. Gonzenbach, A. R. Studart, E. Tervoort and L. J. Gauckler, *Angew. Chem., Int. Ed.*, 2006, **45**, 3526-3530.
- [5] A. Stocco, E. Rio, B. P. Binks and D. Langevin, *Soft Matter*, 2011, **7**, 1260-1267
- [6] Z. P. Du, M. P. Bilbao-Montoya, B. P. Binks, E. Dickinson, R. Ettelaie and B. S. Murray, *Langmuir*, 2003, **19**, 3106-3108.
- [7] E. Dickinson, R. Ettelaie, T. Kostakis and B. S. Murray, *Langmuir*, 2004, **20**, 8517.
- [8] J. Kumaki, *Macromolecules*, 1986, **19**, 2258.
- [9] G. Lagubeau, A. Rescaglio, F. Melo, *Physical Review E*, 2014, **90**, 030201.
- [10] B. Laborie, F. Lachaussee, E. Lorenceau, F. Rouyer, *Soft Matter*, 2013, **9**, 4822-4830.
- [11] R. Aveyard, J. H. Clint, D. Nees and N. Quirke, *Langmuir*, 2000, **16**, 8820-8828.
- [12] D. Y. Zang, E. Rio, D. Langevin, B. Wei and B. P. Binks, *Eur. Phys. J. E*, 2010, **31**, 125-134.
- [13] D. Vella, P. Aussillous and L. Mahadevan, *Europhys. Lett.*, 2004, **68**, 212-218.
- [14] S. S. Datta, H. Cheung Shum and D. A. Weitz, *Langmuir*, 2010, **26**, 18612-18616.
- [15] C. Planchette, E. Lorenceau and A.-L. Biance, *Soft Matter*, 2012, **8**, 2444.
- [16] S. Kam, W. Rossen, *J. Colloid Interface Sci.*, 1999, **213**, 329
- [17] P. A. Kralchevsky, I. B. Ivanov, K. P. Ananthapadmanabhan and A. Lips, *Langmuir*, 2005, **21**, 50-63.
- [18] M. Abkarian, A. B. Subramaniam, S.-H. Kim, R. J. Larsen, S.-M. Yang, H. A. Stone, *Phys. Rev. Lett.*, 2007, **99**, 188301

- [19] C. Monteux, J. Kirkwood, H. Xu, E. Jung, G. G. Fuller, *Phys. Chem. Chem. Phys.*, 2007, **9**, 6344-6350
- [20] von Kármán Th. and Tsien H.-S., *J. Aeronaut. Sci.*, 1939, **7**, 43-50. L. Landau, E. Lifchitz, A. Kosevich, *Théorie de l'élasticité*, Edition MIR, 1990, vol. 7.
- [21] S.B.G. O'Brien, *J. Colloid Interface Sci.*, 1996, **183**, 51-56.
- [22] X. Chateau and O. Pitois, *J. Colloid Interface Sci.*, 2003, **259**, 346-353 ; O. Pitois and X. Chateau, *Langmuir*, 2002, **18**, 9751-9756
- [23] G. B. Davies, T. Krüger, P. V. Coveney, J. Harting., *J. Chem. Phys.*, 2014, **141**, 154902.

[Note1] In the Figure 2 of reference [16], the authors present the ratio $\Delta P/\Delta P_L$ as a function of V/V_p , where V is the gas bubble volume, V_p is the volume of the particles, ΔP is the measured capillary pressure and ΔP_L is the capillary pressure of the equivalent spherical gas bubble of the same volume (V). The two highlighted volume ratios, $(V/V_p)_1$ and $(V/V_p)_2$, correspond respectively to the initial state of our experiment and to the collapse of the bubble. From the figure, it appears that $(\Delta P)_2 = x(\Delta P_L)_2$, with $x < 0$. With these notations, the collapse pressure writes: $\Delta P_{collapse}/(2\sigma/R) = 1 + x(\Delta P_L)_2/(\Delta P)_1$, where $(\Delta P_L)_2/(\Delta P)_1 = \left((V/V_p)_1/(V/V_p)_2\right)^{1/3}$. The ratio a/R is equal to $\left((V_p/V)_1\right)^{1/3}$.

[Note2] In assuming Hertz contacts, the magnitude of the surface pressure is $\Pi \sim Ea^{1/2}\delta\ell^{3/2}/a$, where $\delta\ell$ is the deformation at contact. The magnitude of E_{2d} is $\Pi/(\delta\ell/a)$, so that $E_{2d} \sim Ea(\delta\ell/a)^{1/2}$.

Author contribution statement:

The authors contributed equally to the paper.

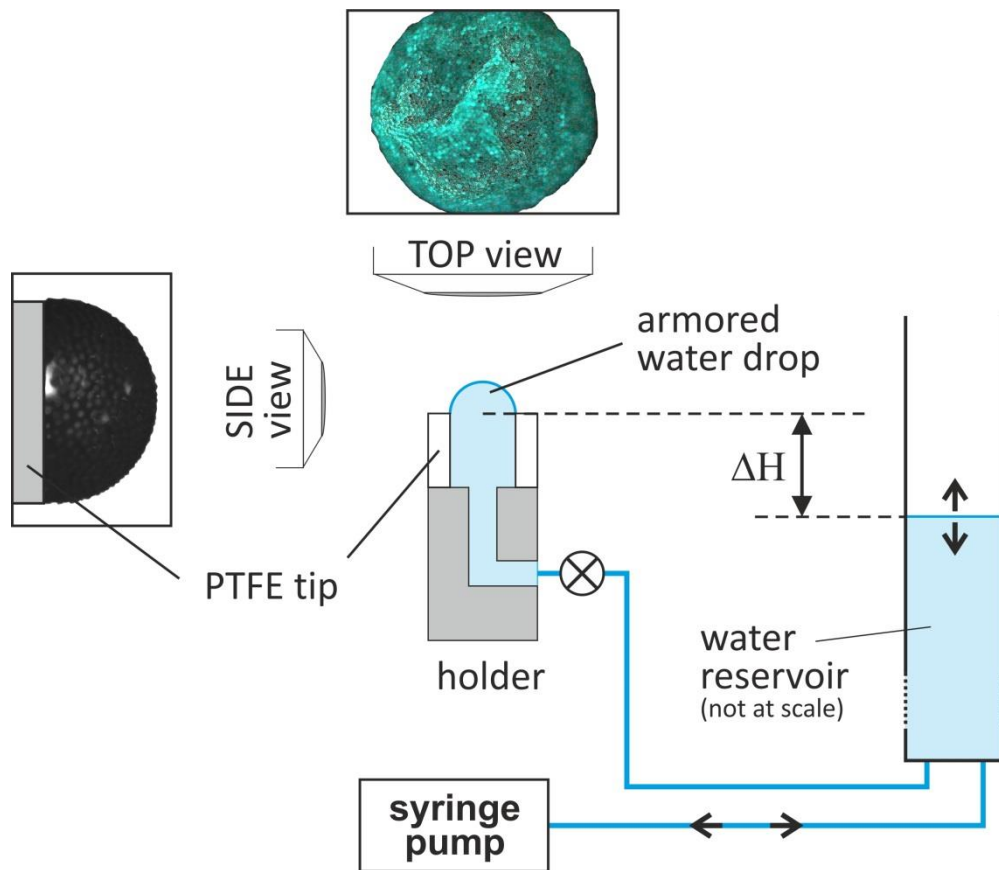


Fig 1: Experimental setup used to measure the collapse pressure of armored water drops subjected to a progressive reduction of their internal pressure.

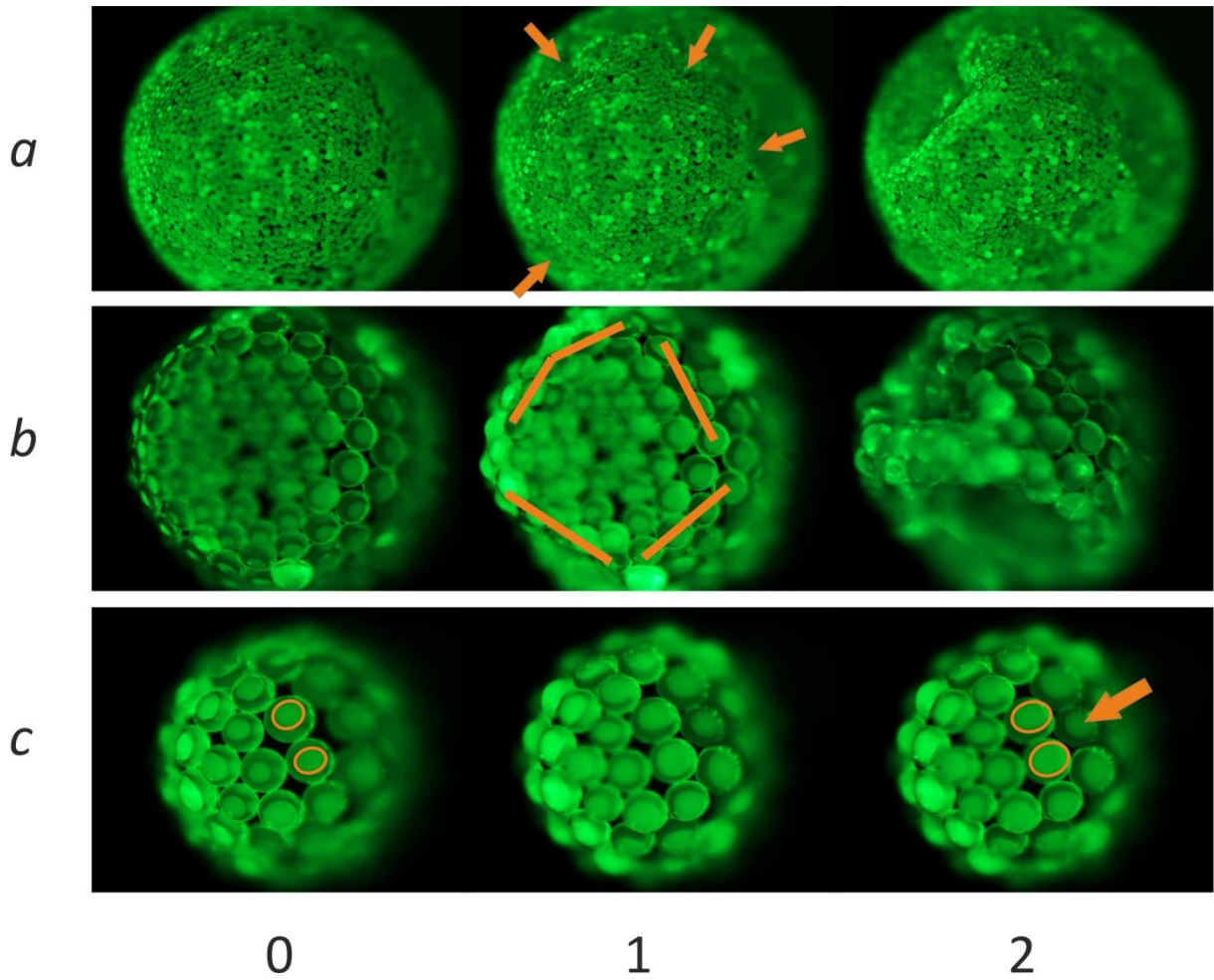


Fig 2: Evolution of the particle armors during the deflation process for three particle-to-drop size ratios: (a) 0.02, (b) 0.12 and (c) 0.17. The columns (0), (1) and (2) correspond to three deflation levels expressed in terms of the ratio $\Delta P/\Delta P_{collapse}$: 0, ≈ 0.9 and ≈ 1 respectively. For column (2), the image has been chosen in order to illustrate the inward buckling responsible for the collapse, but note that for (c2) the collapse is so rapid that the onset of collapse could not be imaged within our experimental conditions. (a1) Note the arrows showing the local inward buckling events. (b1) Note the facets leading to the inward buckling and the drop collapse. The arrow in (c2) shows the particle disentanglement event (refer to the scheme in Fig. 5c) responsible for the drop collapse. Note the evolution of the emerged area on neighboring particles - orange circles in (c0) and (c2) – revealing that those particles are pushed outward of the drop surface.

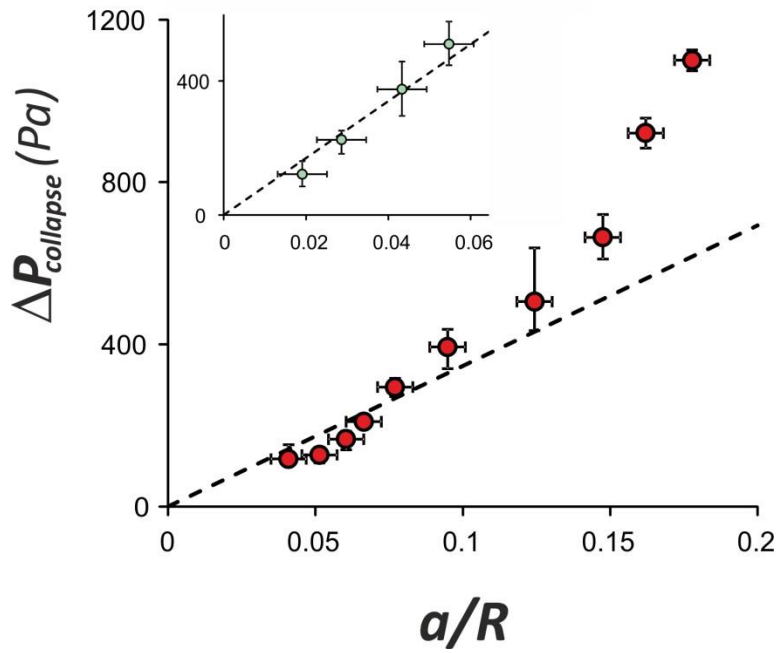


Fig. 3: Measured collapse pressures for armored drops as a function of the particle-to-drop size ratio, for particles with radius 40 μm and 16 μm (in inset). The dashed line gives the initial capillary pressure of the drop (experimental points above this line correspond to negative collapse pressures). Vertical error bars account for deviations (minimal and maximal values) observed for several drops with the same size ratio.

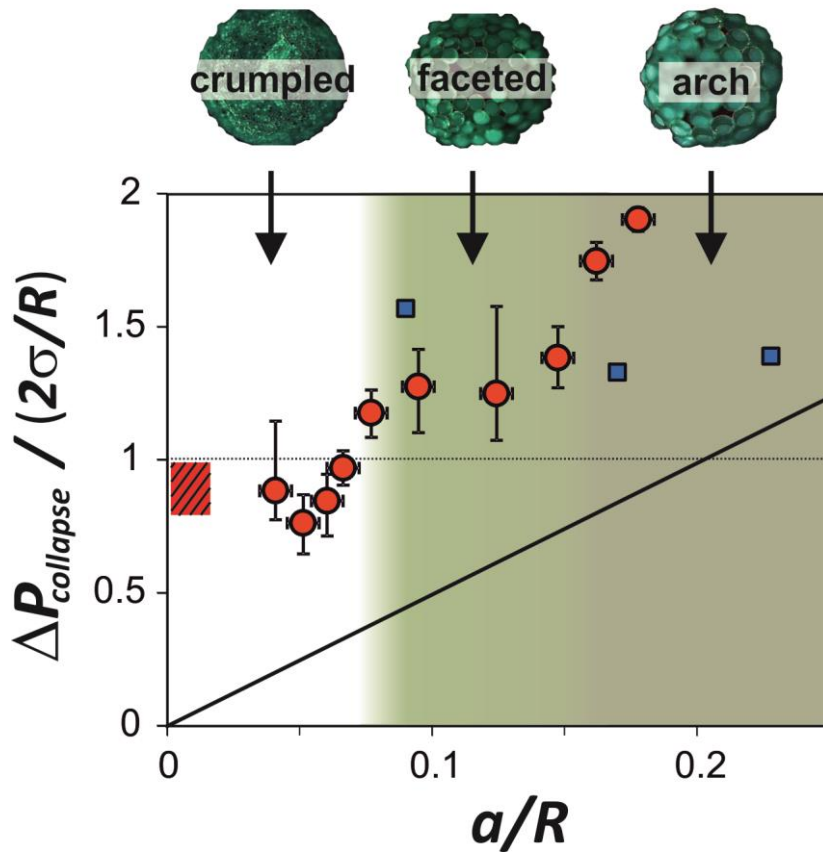


Fig. 4: Link between the morphology of the armored drop before collapse and the measured collapse pressure (red circles). Three morphologies (or regimes) are identified as a function of the particle-to-drop size ratio, namely the ‘*crumpled*’, the ‘*faceted*’ and the ‘*arch*’ regimes. The solid line corresponds to the collapse pressure of elastic shells. The blue squares have been extracted from [18] and correspond to numerical simulations in the ‘*faceted*’ regime. The red hatched area corresponds to collapse pressures reported in [19]. Vertical error bars account for deviations (minimal and maximal values) observed for several drops with the same size ratio.

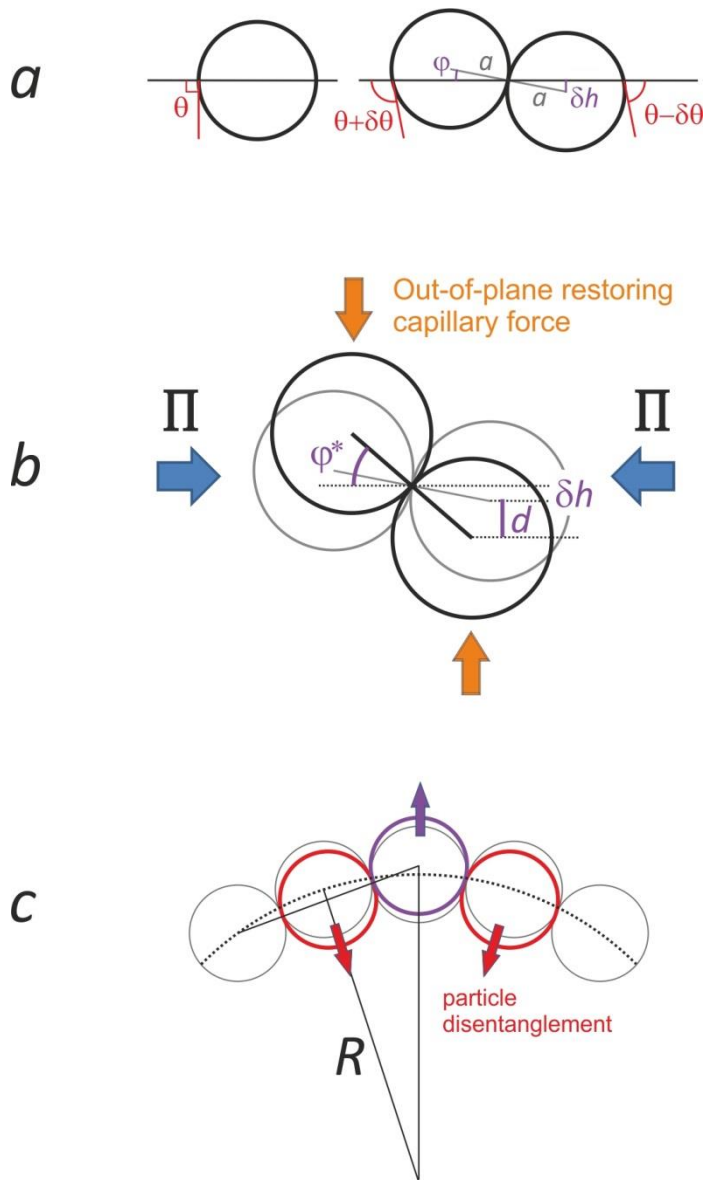


Fig. 5: Behavior of the particles in the armor. (a) Illustration of particle overlapping induced by deviations in the wetting contact angle. (b) The overlapping of the particles increases as the surface pressure increases: particles are pushed perpendicular to the plane of the monolayer and out-of-plane capillary forces develop to ensure the mechanical equilibrium. (c) Illustration of the disentanglement mechanism responsible for the onset of collapse: some particles are pushed outward of the drop surface in order to release enough space in the plane of the armor so that some particles can move inward.